

Experimental evidence of the vapor recoil mechanism in the boiling crisis

V. S. Nikolayev,^{1,2,*} D. Chatain,¹ Y. Garrabos,³ and D. Beysens^{1,4}

¹ESEME, Service des Basses Températures, DRFMC/DSM/CEA-Grenoble,
17 rue des Martyrs, 38054 Grenoble Cedex 9, France

²CEA-ESEME, ESPCI-PMMH-P6-P7, 10, rue Vauquelin, 75231 Paris Cedex 5, France

³CNRS-ESEME, Institut de Chimie de la Matière Condensée de Bordeaux,
Université de Bordeaux I, Avenue du Dr. Schweitzer, 33608 Pessac Cedex, France

⁴CEA-ESEME, ESPCI-PMMH, 10, rue Vauquelin, 75231 Paris Cedex 5, France

(Dated: March 7, 2022)

Boiling crisis experiments are carried out in the vicinity of the liquid-gas critical point of H₂. A magnetic gravity compensation set-up is used to enable nucleate boiling at near critical pressure. The measurements of the critical heat flux that defines the threshold for the boiling crisis are carried out as a function of the distance from the critical point. The obtained power law behavior and the boiling crisis dynamics agree with the predictions of the vapor recoil mechanism and disagree with the classical vapor column mechanism.

Boiling is a highly efficient way to transfer heat. This is why it is widely used, in particular in high power industrial heat exchangers, e.g. nuclear power plant steam generators. Boiling is often considered by the physics community as a well understood phenomenon, at least qualitatively. It is true that boiling has been studied extensively by experiment for common fluids and conventional regimes, for instance for water at atmospheric pressure and moderate heat flux supplied to the fluid. However, the basic theory of boiling remains *terra incognita*, in particular, the phenomena very close to the heating surface, at a scale much smaller than the vapor bubbles [1].

The efficiency of industrial heat exchangers increases with the heat flux. However, there is a limit called Critical Heat Flux (CHF). It corresponds to a transition from nucleate boiling (boiling in its usual sense) to film boiling where the heater is covered by a quasi-continuous vapor film and the evaporation occurs at the gas-liquid interface. Since the gas conducts heat much less than the liquid, the heat transfer efficiency drops sharply during this transition and the heater heats up, which may cause its damage if the power is not cut immediately. This transition is called “burnout”, “departure from nucleate boiling” or “Boiling Crisis” (BC).

Among several dozens of existing models of BC, the Zuber approach [1, 2] is the only one that can be considered as a theory, the others being mainly empirical. According to this model, vapor columns form at the nucleation sites on the heater. The vapor moves upwards while the liquid moves to the bottom of the column where evaporation occurs. This counter-flow motion induces the Kelvin-Helmholtz instability, which leads to the destabilization of the whole system and to the creation of a vapor film on the heater. The transition occurs when the vapor velocity exceeds a threshold [2] resulting in the following CHF expression,

$$q_{CHF} \sim H[\sigma g(\rho_L - \rho_V)\rho_V^2]^{1/4}, \quad (1)$$

where H is the latent heat, ρ_L (ρ_V) is the density of the liquid (gas) phase, σ is the surface tension, and g is the gravity acceleration. While this expression fits a number of experimental data sets, the underlying physics is questionable. Indeed, the vapor column morphology of boiling is quite rarely observed while the BC exist for almost all morphologies of boiling, for pool boiling (i.e., natural convection boiling) or for flow boiling (i.e. boiling of the fluid flowing in a heated tube). Besides, many experimental results, in particular those obtained in low-gravity [3], cannot be fitted by Eq. (1). Other physical phenomena should then be responsible for the triggering of BC. A strong dependence of CHF on the wetting properties of the heater [1] suggests a phenomenon at the contact line level.

A vapor recoil mechanism for BC has already been proposed in [4, 5]. A fluid molecule leaving the liquid interface causes a recoil force analogous to that created by the gas emitted by a rocket engine. It pushes the interface towards the liquid side in the normal direction. An average vapor recoil force appears because the fluid necessarily expands while transforming from the liquid to the gas phase. The stronger the mass evaporation rate η (per time and interface area), the larger the vapor recoil force. One finds that the vapor recoil force per interface area is $P_r = \eta^2(\rho_V^{-1} - \rho_L^{-1})$ [4]. The evaporation is particularly strong in the vicinity of the contact line of a bubble, inside the superheated layer of the liquid (Fig. 1). The resulting vapor recoil force can pull apart the bubble contact line and make it spread over the heater, thus creating a nucleus for the vapor film. The results of the vapor recoil model are in qualitative agreement with the observations by some of us [6] and those by other groups [7, 8]. The present Letter deals with its quantitative verification.

Consider the fluid far from its critical point, where the system pressure $p \ll p_c$ (p_c is the critical pressure). Instead of using pressure, it is more convenient to argue in terms of the saturation temperature T from which p can

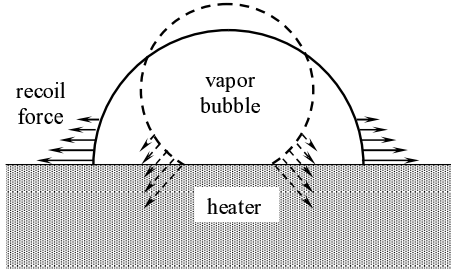


FIG. 1: Sketch illustrating how the vapor recoil initiates the bubble spreading. The amplitude and direction of the vapor recoil force are shown by arrows.

be obtained readily. An estimation [4] shows that the heat flux necessary to create a vapor recoil force comparable to that of the surface tension corresponds to the experimental CHF order of magnitude. If the contributions of the vapor recoil and the surface tension σ are of the same order,

$$\frac{P_r l_c}{\sigma} \sim \frac{q_{CHF}^2 l_c}{H^2 \sigma} \left(\frac{1}{\rho_V} - \frac{1}{\rho_L} \right) = \text{const}, \quad (2)$$

where the capillary length $l_c = \sqrt{\sigma/g(\rho_L - \rho_V)}$ is the natural lengthscale. Eq. (2) results in a CHF expression identical to Zuber's expression (1) if the inequality $\rho_L \gg \rho_V$ is taken into account. Both models are then difficult to distinguish far from the critical temperature T_c .

On the contrary, their behaviors close to T_c are quite different. A reasoning presented in [6] led to the following vapor recoil model result

$$q_{CHF} \sim (T_c - T)^{1+\nu-3\beta/2}, \quad (3)$$

where $\beta = 0.325$ and $\nu = 0.63$ are the universal critical exponents, $1 + \nu - 3\beta/2 = 1.14$. The Zuber expression (1) also leads to a power law with exponent $5\beta/4 + \nu/2 = 0.72$. This value can be obtained from the scaling relations $H \sim \rho_L - \rho_V \sim (T_c - T)^\beta$ and $\sigma \sim (T_c - T)^{2\nu}$.

The thermal diffusivity vanishes at T_c . The thermally controlled bubble dynamics is thus slower than at low pressure (critical slowing down) and the CHF is much smaller. Optical distortions inevitable at low pressures because of violent fluid motion and strong temperature gradients [9] are nonexistent at $T \simeq T_c$ where very detailed observations can thus be performed. However, the surface tension becomes very low and gravity flattens the gas-liquid interface. Reduced gravity conditions are thus necessary to preserve the existence of bubbles, hence the nucleate boiling itself.

The cryogenic magnetic levitation installation at CEA-Grenoble [10] was used to achieve a gravity compensation. The accuracy is of 2% in the cylindrical fluid volume of 8 mm diameter and 5 mm thickness. The experimental cell (Fig. 2) can be partially filled or pumped off *in situ*

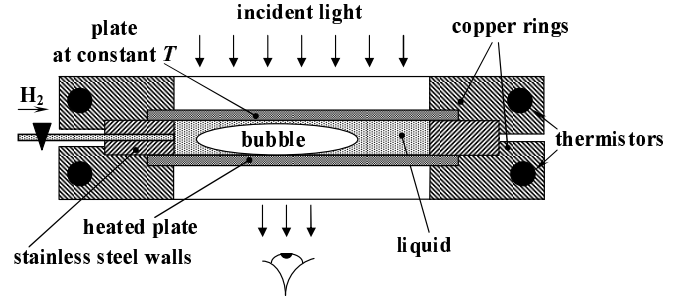


FIG. 2: Sketch of the cylindrical transparent experimental cell.

by using a capillary equipped with a cryogenic electric valve. The latter remains closed during the experiment. The cell is filled with H_2 at critical density ρ_c so that the gas phase occupies a half of the cell independently of T because of the symmetry of the co-existence curve with respect to ρ_c , $(\rho_L + \rho_V)/2 = \rho_c$. During the evolution, the bubble mass can vary while its volume does not change.

The best observations of BC [2, 7, 8, 11–13] involved a transparent heater to detect and follow the heater dry-out. Our cylindrical cell (Fig. 2) has transparent sapphire end plates. Several thermistors are integrated into copper rings that have a good thermal contact with the plates. Both rings are connected thermally to a colder liquid helium bath with wires that serve as thermal resistances. The thermistors are used to inject the controlled heat power into one of the plates that serves as a heater and to maintain the temperature of the other plate with 1 mK precision (in a stationary state) by a temperature regulation system. Sapphire is an excellent heat conductor in the cryogenic temperature range ($T_c = 33\text{K}$ for H_2). The lateral cell wall is made of stainless steel, with conductivity about 10^3 times less than that of the sapphire.

Because of the complete wetting conditions characteristic of near critical fluids [6], the wetting layer always covers the cell at equilibrium. Due to this fact, a good thermal contact of the temperature controlled plate with the rest of the fluid is provided. The cell location with respect to the magnetic field is chosen in such a way that a residual magnetic force (which plays the role of an effective gravity) positions the bubble against the heating plate. This effective gravity field is directed to the cell center ([10], see also the sketch in Fig. 5a below) so that the denser liquid phase is attracted to the cell center. Unfortunately, it is quite difficult to quantify the force acting on the bubble since there is no possibility to map the magnetic field with a sufficient precision.

The surface tension prevents the liquid from gathering in the cell center by keeping the bubble convex, and the bubble image is circular far from T_c . Close to the critical point, the surface tension becomes too weak and the liquid gathers in the center. Since the wetting layer

remains at the cell walls, the bubble takes an unusual torus shape, see Fig. 5. This occurs at $T = T_g \approx 32.9\text{K}$. We call this geometry annular because of the observed bubble image.

For each experimental run, a thermal regulation reference temperature is chosen and defines T . By tuning the heater power, the cell is thermally equilibrated. Then heating is increased as needed and a stationary boiling state is obtained after a transition period. The heater power P and the heater temperature T_h are then recorded.

T_h has been measured also with the empty cell for different T and heating powers P_e and the dependence $P_e = P_e(T_h, T)$ was established. The amount of heat transferred across the cell walls of the filled cell can thus be determined by calculating this function for the values of both temperatures measured in the filled cell. The heat flux q carried by the fluid is obtained by dividing $P - P_e$ by the heater area. The dependence of q (calculated as explained above) on T_h is called the boiling curve (Fig. 3).

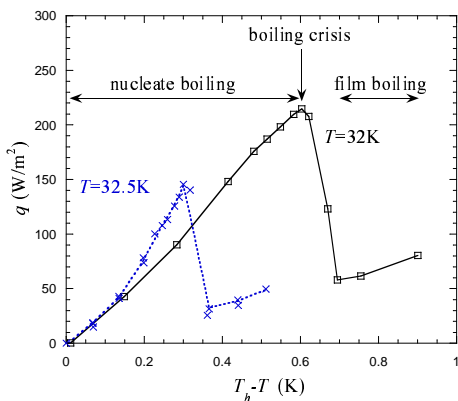


FIG. 3: Examples of the boiling curves for different pressures corresponding to two indicated values of T . The boiling regimes are indicated (32K curve). The lines are guides for the eye.

The cell can be observed optically through the plates by using a light source, a CCD camera and two periscopes. Far from T_c , the bubble is circular (Fig. 4). The nucleation, growth and departure of small gas bubbles occur at the periphery of the heating plate where the liquid wetting layer is thicker. Since the large bubble occupies most of the plate image and its curved surface looks dark, the small bubbles are almost invisible. Their presence can be detected by the trembling of the large bubble during their coalescence. A sudden disappearance of the trembling indicates the complete dryout of the liquid film (Fig. 4c). The nucleation of the dry spot and the contact line motion is difficult to observe in this geometry without special optical means [14]. At $T \lesssim T_g$ the wetting layer thickens and the contact line becomes visible in motion but the optical contrast is low.

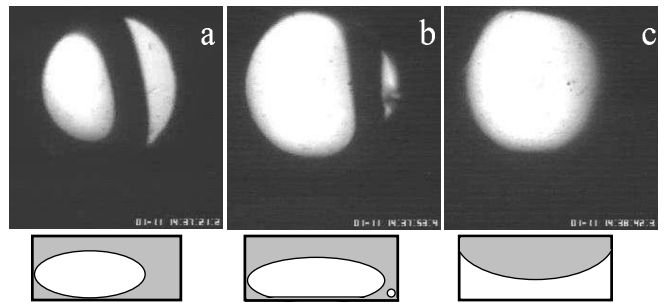


FIG. 4: Heater drying dynamics at the CHF at $T = 32.5\text{K}$ visualized through the transparent heater (closest to the observer). (a) Initial bubble position at equilibrium. (b) Bubble partially spread. (c) The heater is completely dried out. The section of the cell interior with a plane perpendicular to the image is sketched below the corresponding photo. On the sketches, the vapor is white and the liquid is gray; the heater is at the bottom.

At the CHF the BC does not occur immediately after the temperature rise. The cell first attains a nearly stationary state where T_h fluctuates slightly. One of the fluctuations then leads to a rapid drying of the major part of the heater. At the CHF, the liquid loses completely its contact with the heater which corresponds to film boiling. The transferred heat flux q falls sharply (Fig. 3). Practically no fluid motion is observed any more even when the heating power is increased.

The optical contrast is much better in the annular regime ($T_g < T < T_c$) because the wetting layer is several times thicker. Its thickness can be judged from the maximum size of small bubbles that nucleate and grow inside it (Figs. 5a,b). Small bubbles also form in the plate cen-

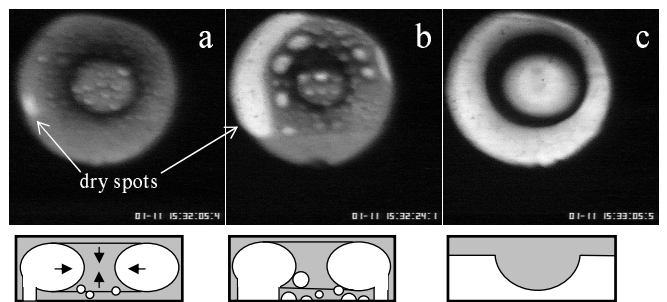


FIG. 5: Heater drying dynamics slightly above the CHF at $T = 32.95\text{K}$ (in annular geometry, the large bubble has a toroidal shape as described in the text). The bright areas on the photos are the dry spots. Similarly to Fig. 4, phase distributions for each photo are shown in the sketches. (a) Beginning of the dry spot (small white spot to the left) growth. (b) Intermediate stage. (c) Complete drying of the heater; the liquid phase has taken a shape of a hat seen from the top. Nucleated small bubbles are visible in (a-b). The direction and the relative magnitude of the effective gravity are shown by arrows in the sketch (a).

ter, which is convenient for their observation. They grow

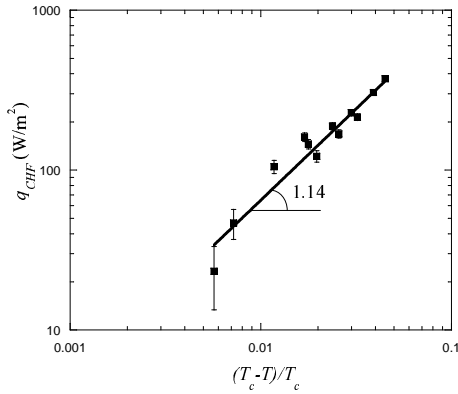


FIG. 6: The critical heat flux as a function of the distance to the critical point. The solid straight line is the vapor recoil model prediction Eq. (3).

and slide to the plate periphery or depart from the plate under the action of the effective gravity, which pushes them in the direction of the large bubble. They eventually coalesce with it.

At $q \lesssim q_{CHF}$ dry spots under the small bubbles begin to appear and disappear intermittently when the bubbles depart from the heater. A bubble that appears in the hottest point (where the liquid layer is thinner, presumably due to the vapor recoil pressure) coalesces with the toroidal bubble and forms a dry spot which remains stationary. This bubble forms intermittently a “bridge” connecting the large bubble to the heater as sketched in Fig. 5a. At $q = q_{CHF}$ a large dry spot also appears (Fig. 5a) and keeps growing (Fig. 5b). The smaller dry spots under other bubbles keep appearing and disappearing but grow larger. All the dry spots grow so large that they coalesce and, suddenly, the heater dries out completely (Fig. 5c). This picture is in full analogy with the observations by other groups [7, 8] performed at much lower pressures. As expected, the BC slows down near T_c , and can take as long as 1-2 min for the closest to T_c runs.

The thickness of the wetting layer reflects the force that presses the bubble against the heater. When the layer is thicker (smaller force), a larger heat flux is needed to dry out the heater and the CHF is larger. This is what happens after a cell displacement with respect to the magnetic field or after a bubble topology change. The $q_{CHF}(T)$ dependence should thus be measured at the same (circular) bubble topology, i.e. at $T < T_g$.

The $q_{CHF}(T)$ dependence is shown in Fig. 6 and compared with the vapor recoil model prediction, Eq. (3). A good agreement is found, which demonstrates the validity of the model. It is evident that the data cannot be fitted

well with the Zuber equation (1) as the corresponding slope is nearly twice smaller.

The boiling crisis has been observed at high, nearly critical pressure and at low gravity. At these conditions the BC is triggered by the growth of dry spots under individual vapor bubbles and is qualitatively analogous to the BC at normal gravity and low pressures. The dry spot growth is followed by the bubble coalescence provoking heater dryout. At low pressures, the vapor recoil model gives a CHF expression similar to the classical Zuber formula. At high pressures, the two expressions, however, differ strongly. The measurements of the CHF depending on the distance to the critical point demonstrate the validity of the vapor recoil model.

These results open the way to more precise numerical simulation that can now be based on a well identified physical phenomenon. The CHF can then be predicted as a function of various system parameters such as pressure, material properties, geometry, gravity level, etc.

This work is partially supported by CNES. We thank D. Communal for his contribution to the thermal regulation system and P. Seyfert for his helpful comments.

* Web page: <http://www.pmmh.espci.fr/~vnikol>

- [1] V. K. Dhir, *Annu. Rev. Fluid. Mech.* **30**, 365 (1998).
- [2] T. G. Theophanous, T. H. Dinh, J. P. Tu, & A. P. Dinh, *Exp. Thermal Fluid Sci.* **26**, 793 (2002).
- [3] J. Straub, *Adv. Heat Transfer* **35**, 57 (2001).
- [4] V. S. Nikolayev & D. A. Beysens, *Europhys. Lett.* **47**, 345 (1999).
- [5] V. S. Nikolayev, D. A. Beysens, G.-L. Lagier, & J. Hegseth, *Int. J. Heat Mass Transfer* **44**, 3499 (2001).
- [6] Y. Garrabos, C. Lecoutre-Chabot, J. Hegseth, V. S. Nikolayev, D. Beysens, & J.-P. Delville, *Phys. Rev. E* **64**, 051602 (2001).
- [7] S. G. Kandlikar & M. E. Steinke, *Int. J. Heat Mass Transfer* **45**, 3771 (2002).
- [8] S. Nishio, H. Tanaka, *Int. J. Heat Mass Transfer* **47**, 4559 (2004).
- [9] D. B. R. Kenning, *Int. J. Heat and Fluid Flow* **25**, 209 (2004).
- [10] D. Chatain & V. S. Nikolayev, *Cryogenics* **42**, 253 (2002); Wunenburger R., Chatain D., Garrabos Y., Beysens D., *Phys. Rev. E* **62**, 469 (2000).
- [11] H. J. van Ouwkerk, *Int. J. Heat Mass Transfer* **15**, 25 (1972).
- [12] K. Torikai, K. Suzuki & M. Yamaguchi, *JSME Int. J. Series II* **34**, 195 (1991).
- [13] D. Jamet, O. Lebaigue, private communication (2006).
- [14] J. Hegseth, A. Oprisan, Y. Garrabos, V. S. Nikolayev, C. Lecoutre-Chabot & D. Beysens, *Phys. Rev. E* **72**, 031602 (2005).